Scientific paper

Optical Analysis of Hafnium Oxide-aluminum Multilayer Structures for Transparent Heat Mirrors

Muhammad Ramzan,[1,*] Anwar M. Rana,[1] Muhammad Hafeez,[2] Ejaz Ahmed,[1] Arshad S. Bhatti,[2] Muhammad F. Wasiq[3] and Muhammad Y. Nadeem[1]

[1] *Department of Physics, Bahauddin Zakariya University, Multan-60800, Pakistan.*

[2] *Center for Micro and Nano Devices (CMND), Department of Physics, COMSATS Institute of Information Technology (CIIT), Islamabad-44000, Pakistan.*

[3] *Computer Engineering Services, Chughtai Plaza, 35-Blue Area, Islamabad, Pakistan.*

* *Corresponding author: E-mail: mrkhawar81@yahoo.com*

Received: 13-09-2013

Abstract

We report on HfO_2/*Al*/HfO_2 multilayer thin films for heat mirror applications prepared on corning glass substrates by electron beam evaporation. Films fabricated at a substrate temperature of 100 °C show nano-polycrystals of HfO_2 embedded in a disordered lattice according to X-ray diffraction results. Atomic force microscopy revealed that HfO_2/*Al*/HfO_2 layers possess smooth surface that is appropriate for optical heat mirror applications. Study of optical properties by UV-Visible spectrophotometer demonstrated that transmittance of HfO_2/*Al*/HfO_2 device was decreasing from UV to VIS and then slightly increasing in the NIR regions, with an opposite trend followed by reflectance. Optical constants i.e. refractive index, extinction coefficient, band gap energy, Urbach energy has also been calculated. The optical band gap and Urbach energy are found to be 4.34 eV and 3.164 eV, respectively. The collective oscillation energy loss for heat mirrors applications are also observed.

Keywords: Optical properties, D/M/D multilayer thin films, X-ray diffraction, Atomic force microscopy, Transparent heat mirrors.

1. Introduction

Amorphous thin films are interesting materials and attractive in the fields of optical recording and integrated optics such as all-optical switches, gratings and waveguides. Transition metal oxides have shown unique features for various applications such as biosensors, gas sensors, catalyses, electrochromic windows, energy-efficient windows, fuel cell membranes, and lithium-ion batteries.[1–4] A transparent heat mirror (THM) has high visible transmittance ($400 < \lambda < 700$ nm) and high infrared (IR) reflectance ($700 < \lambda < 3000$ nm), λ being wavelength of light. These mirrors are used in flat-plate collectors for solar heating/cooling, and on windows for thermal insulation of buildings.[5] Due to high free electron density metals show high reflectance through IR and visible ranges. Free-electron-like metals, such as silver, gold, aluminum, copper, nickle etc. have been selected for THM applications.[6–8] To further enhance visible transmittance of metallic films, dielectric-metal-dielectric (D/M/D) multilayer coatings are used. The dielectric layer first acts as anti-reflection coating to enhance the reflectance. Secondly it improves the acceptability of the effective transition wavelength and range. Moreover, it contributes to destructive interference of the reflected light in the visible range.[6] Thirdly it protects the metallic layer from environmental effects such as abrasion and corrosion. Finally, bottom dielectric provides a nucleation modification layer, which enhances the growth of a continuous thin film.[9] Such a three-layer structure allows broad band reflectance and flexibility in band pass selection as single metallic films do not offer the stability and durability for practical heat mirrors. [8,10] Aluminum has superior properties for THM applications as it is highly effective barrier to the ravages of air, tempe-

rature, moisture, and chemical attack. Electron beam evaporation has been used for deposition of present films as it involves precise control of deposition rates, excellent material utilization and freedom from contamination etc.[11] Hafnium oxide (HfO_2) is an important material due to its present and future applications in microelectronics.[12–15] Its wide bandgap (~5.5 eV, [16]) gives its transparency over a wide spectral range making it useful in optical coatings.[17] Heat mirror based on HfO_2 using Ag reflective layer was fabricated by Al-Kuhaili [18] which showed average transmittance of 72.4% and an average reflectance of 67.0% in the NIR region (700–2000 nm). Moreover, HfO_2/M/HfO_2 heat mirrors (with M = Hf, Mo, *Al*) were also fabricated by Selvakumar *et al.* [19,20] using magnetron sputtering system. They observed high solar absorptance of 90.5–92.3% (for HfO_2/Mo/HfO_2) and 91.6–92.5% (for HfO_2/Hf or *Al*/HfO_2) heat mirrors which show a decrease in absorptance on annealing up to 500 °C. They also noted that HfO_2/*Al*/HfO_2 heat mirrors were thermally stable in air up to 350 °C for 2 hours. In this work, HfO_2 layers are formed on both sides of *Al* film to reflect light from metal surface as a HfO_2/*Al*/HfO_2 device. Structural, morphological and optical properties of this multilayer structure are reported for transparent heat mirror applications.

2. Experimental

Corning glass substrates (dimensions 75 × 25 mm^2, thickness ~0.96–1.06 mm) were ultrasonically cleaned using acetone, IPA and Piranha solution [H_2SO_4:H_2O_2(30%)] before deposition and kept at 100 °C during deposition. Metal film of ~5 nm thickness was deposited from 99.98% pure aluminum wire (Φ = 1.5 mm) and sandwiched between two dielectric layers (each ~10 nm thick) formed by granular HfO_2 (99.95% pure) using graphite crucible under vacuum (>10^{-5} mbar) in electron-beam evaporator (BOS Edward AUTO500). To minimize evaporation-introduced roughness during deposition, low evaporation rates were maintained at 0.0069 nm s^{-1} for dielectric and 0.1388 nm s^{-1} for metal layers. Film thickness and deposition rate were monitored by quartz crystal monitor (Edward FTM7). The actual film thickness was measured by optical methods using spectroscopic ellipsometry. The difference of these two measurements was in the range of ± 1 nm. Various deposition parameters are listed in Table 1. Crystal structure of these films was investigated through X-ray diffraction (XRD) patterns recorded at room temperature using PANalytical's X' Pert PRO diffractometer equipped with Cu K_α radiations in the 2θ range from 20–80°. The surface topographical modifications of thin multilayer films were investigated by Agilent 5100 atomic force microscopy (AFM) in contact mode. A sample area of (2 × 2 μm^2) was scanned by a silicon tip having radius in the range from 5–10 nm with a frequency of 0.5 Hz. The substrates were not damaged by scanning the silicon AFM tip onto them. This was demonstrated by scanning the tip several times after which no change in the AFM topographic images was observed. Statistical analysis of AFM images and distribution of grain size (by the watershed technique) was carried out using Gwyddion software (Gwyddion 2.29, GNU General Public License, http://www.gwyddion.net, 2012). Optical properties of HfO_2-*Al*-HfO_2 devices were determined using Perkin-Elmer Lambda 9 UV/Vis/NIR spectrophotometer. For reflectance measurements a separate assembly was inserted in the spectrophotometer and has not been evaluated using R + T + A =1.[21]

Table 1: Deposition Parameters of HfO_2/*Al*/HfO_2 multilayer thin films.

Crucible	Graphite
Substrate	Corning Glass
Sample Thickness	25 nm
Chamber Pressure	5.0×10^{-5} mbar
Substrate Temperature	100 °C
Deposition Time	18:35 min
Deposition Rate (For *Al*)	0.1388 nm s^{-1}
Deposition Rate (For HfO_2)	0.0069 nm s^{-1}

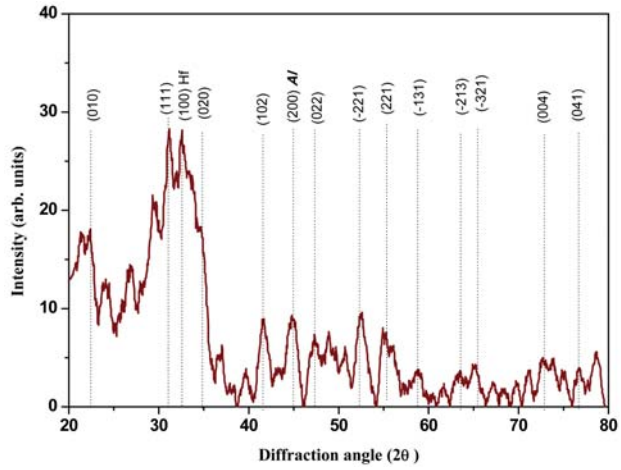

Fig. 1: X-ray diffraction pattern for HfO_2/*Al*/HfO_2 multilayered films.

3. Results and Discussion

3. 1. Structural Characteristics

Fig. 1 shows XRD pattern of HfO_2/*Al*/HfO_2 device. A broad diffraction peak between 25 and 35° (involving diffraction peaks (111) and (020) for HfO_2 and (100) of α-Hf in Fig. 1) indicates amorphous/disordered nature of the device.[11] However, the observed diffraction peaks have been indexed and identified using JCPDS ref. 06–0318 corresponding to HfO_2 monoclinic structure [space group P21/c, lattice parameters; a = 5.12 Å, b = 5.18 Å and c = 5.25 Å],[22]

JCPDS ref. 38–1478 for α-Hf (hexagonal), and JCPDS ref. 04–0787 for *Al* (cubic). Almost all the diffraction peaks of HfO_2 and α-Hf are weak and broader which lead to polycrystalline multiphase and nano-sized grains.[11, 23] The strongest line at $2\theta = 32°$ is indexed as HfO_2 (111). It is noticed that diffraction intensity drops on increasing incident angle, resulting in a steep penetration depth into the substrate. The polycrystalline nature of HfO_2 is consistent with its crystallization kinetics on glass and for transparent heat mirrors.[24] Presence of metallic intermediate layer provoked the crystallization of oxide (HfO_2) layer.[25] Since crystallinity in D/M/D films is influenced by the microstructure and purity of an intermediate layer.[26] However, *Al* insertion deteriorates crystallinity of the devices which may cause stress formation as a result of the ion-size difference between *Al* and Hf ($r_{Al} = 0.054$ nm and $r_{Hf} = 0.071$ nm).

3. 2. Surface Characteristics

Fig. 2(a) displays two and three-dimensional AFM micrographs (2 μm × 2 μm) of HfO_2/*Al*/HfO_2 structure. Tightly packed slightly elongated grains having an average grain size of 11.9 nm (as determined by watershed technique using Gwyddion software), good homogeneity and no cracks are clearly visible. Microroughness of thin films is an important parameter for the development of optical coatings especially in the UV region for applications such as lithography and heat mirrors.[24] For characterization of an optical surface (coatings) the root-mean-square (RMS) roughness is normally used. AFM data used for roughness measurements using Gwyddion software revealed quite a smooth surface having average RMS roughness of 3.83 ± 0.42 nm obtained from several scans. The RMS roughness can also be determined from the height distribution as depicted by Fig. 2b(I). The height distribution seems to be symmetric. Moreover, the above roughness obtained from the AFM image is the convolution of the shape and local roughness of the island.[27] As the height distribution becomes increasingly broadened, it indicates a rougher surface. The root-mean-square roughness can be expressed as height distribution using following relation: [28]

$$R_q = \sqrt{\frac{1}{N}\sum (z_i - \bar{z})^2} \quad (1)$$

where **N** is the total number of height measurements, z_i is each height value, and $\bar{z}$ is the mean height. In addition, the

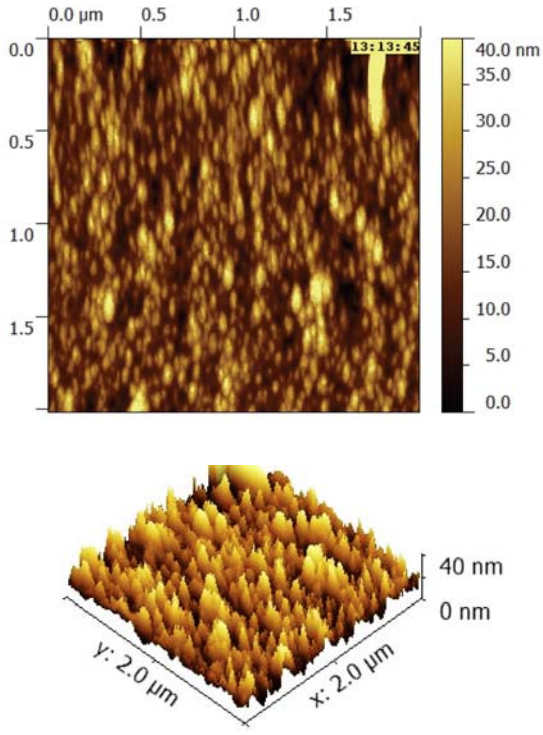

Fig. 2(a): Two- and three-dimensional AFM images of Hf-O_2/*Al*/HfO_2 device with a scan area of 2 × 2 μm^2.

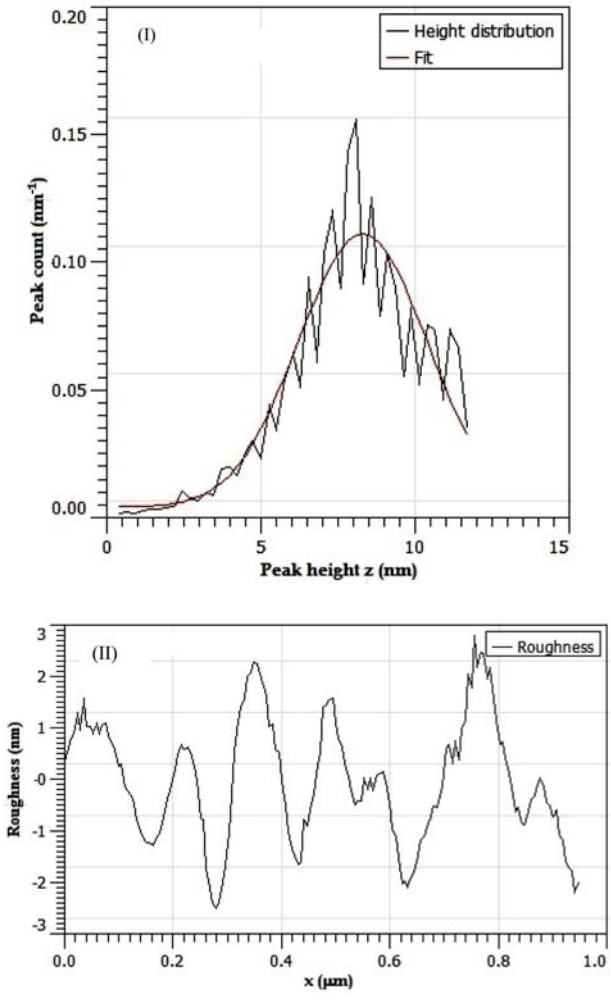

Fig. 2(b): Various roughness parameters as determined from AFM images of HfO_2/*Al*/HfO_2 device such as: (I) height distribution showing peak count as a function of peak height along with Gaussian fit to data, and (II) RMS roughness as a function of position x.

positive low value of skewness (R_{sk} = 0.236 ± 0.016) shows that peaks are slightly dominant on the surface, whereas the kurtosis value (R_{ku} = 2.517 ± 0.244) indicates that the distribution of grains over the scanned area has relatively few high peaks and low valleys which signifies a slightly bumpy surface.[29] Moreover, Fig. 2b(II) shows that the asperities and depressions observed at various positions on the surface of multilayer films are of the order of 2–6 nm wide. Low values of surface roughness of the device with *Al* insertion may be due to *Al* presence at disordered regions in the boundary.[23] Such low roughness values satisfy the requirements of general heat mirrors sufficiently.

3. 3. Optical Characteristics

Fig. 3(a) represents transmittance spectra for HfO_2/*Al*/HfO_2 device in the wavelength range of 250–2500 nm. Optical transmittance of HfO_2 films is mostly confined to UV-visible region (91%) but reduces to 42% at ~ 550 nm and then slowly increases in the NIR region up to ~ 55%. Reflectance for HfO_2/*Al*/HfO_2 device has been measured exposing both coated and uncoated sides of the substrate to the incident beam as shown in Fig. 3(b).

First plot of Fig. 3(b) depicts very weak optical reflectance (%R-coated) of the device in the UV range, whereas it rises suddenly in the visible and NIR regions due to influence of intermediate *Al* metallic layer with a maximum (~60%) at ~ 1050 nm. Second plot (%R-uncoated) in Fig. 3(b) shows reflectance variations of HfO_2/*Al*/HfO_2 device measured from uncoated side of the substrate. In this case, reflectance is found to be high up to 30% in the visible and (20–25%) in the NIR regions. For warm climates ideal heat mirrors allow visible energy to transmit through the window, while reflecting majority of all IR energies including that of sun from the window.[30] Heat mirror (HfO_2/Ag/HfO_2) fabricated by Al-Kuhaili[18] using Ag reflective layer showed average transmittance of 72.4% in visible region and an average reflectance of 67.0% in the NIR region

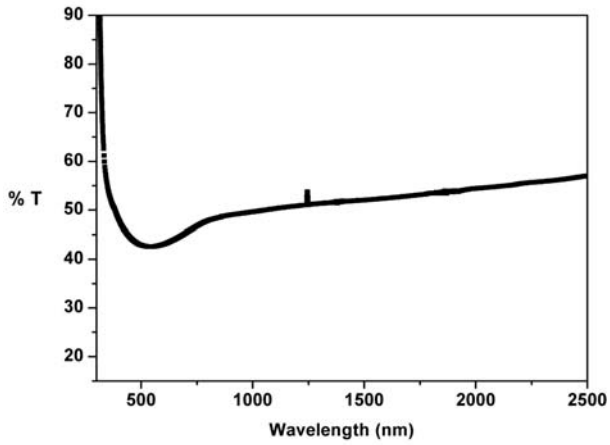

Fig. 3(a): Optical transmittance 'T' Vs. wavelength plot for HfO_2/*Al*/HfO_2 device.

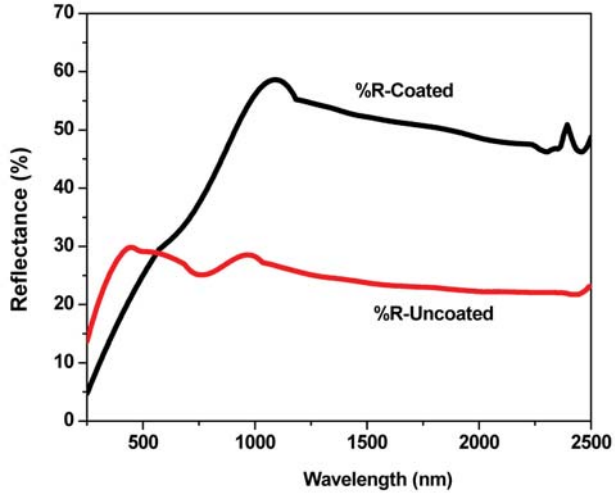

Fig. 3(b): Spectral reflectance of HfO_2/*Al*/HfO_2 device measured from coated and uncoated sides of the substrate.

(700–2000 nm). Present results are in close match with those of Kuhaili.[18] The relatively low values of reflectance in the NIR region is due to slight rise of transmittance of present *Al*-based device as compared to Ag-based device (which shows weak transmittance in this region). Further research work on present *Al*-based device is in progress to optimize the device for optimal properties. Moreover, the plasma wavelength is near a wavelength at which the reflectance shows a minimum.[31] For present HfO_2/*Al*/HfO_2 devices the plasma wavelength is very short as reflectance is minimum in the UV region (Fig. 3b). Since short plasma wavelength and high IR reflectance are two prerequisites for heat mirrors. Such optimized optical properties of HfO_2/*Al*/HfO_2 structure could be useful in some applications as heat mirrors and/or as transparent conductive oxides.

Refractive index 'n' is determined from reflectance (*R*) spectrum (Fig. 3b) using following relation: [23]

$$n = \frac{1+\sqrt{R}}{1-\sqrt{R}} \qquad (2)$$

The resulting dispersion curve shown in Fig. 3(c) depicts the highest value of n in visible region, i.e. n = 3.29 at λ = 632.8 nm. Such value of refractive index is significantly higher than that of bulk HfO_2 (2.08,[22]) at the same wavelength. This rise in n indicates a density change in the device, which corresponds to a decrease in film porosity. AFM results support these findings. Moreover, polycrystalline multi-phase nature and disorderness in HfO_2/*Al*/HfO_2 device (as depicted by XRD spectrum) may also cause rise of n values. Refractive index for the amorphous/disordered phase was found to be high as compared to polycrystalline one.[15,32] In addition, there is a gradual decrease in n values to ~2.03 in the NIR region, which may be attributed to gradual fall in reflectance. The optimization of IR reflectance should

have to be considered so that it rises to about 85% instead of decreasing since commercial heat mirrors usually have visible transmittance not less than 85% and IR reflectance around 85%.[33]

To determine complex refractive index from optical spectra, not only real part *n* is obtained, but also the imaginary part or extinction coefficient *k* given by:[23]

$$k = \frac{\lambda}{4\pi d} \ln\left(\frac{1-R}{T}\right) \quad (3)$$

where *d* is the thickness of HfO_2/*Al*/HfO_2 device. Plot of *k* vs. wavelength λ shown in Fig. 3(c) indicates minimum absorption in visible region. Throughout visible region, *k* is almost low showing very small optical loss in this region, which is a desirable property for dielectric layers in a transparent heat mirror. However, *k* rises in IR region which could be related to the existence of large amount of defects originating from oxygen vacancies as evidenced by XRD illustrating the presence of Hf phase lacking oxygen in HfO_2/*Al*/HfO_2 device.

Fig. 3(c) also shows energy loss function to portray the energy of collective oscillations in HfO_2/*Al*/HfO_2 defined as:[34]

$$\text{Im } \varepsilon^{-1} = 2n\,k/(n^2 + k^2) \quad (4)$$

The sharp rise in energy loss function, Im ε^{-1}, (Fig. 3c) shows consequent locations where collective oscillation takes place. It gives an accurate position for the interband transition and relative energy loss of *Al* films. The loss function consequently shows peaks at the wavelength range 250–2500 nm.

Spectral dependence of absorption coefficient (α) in the region of fundamental absorption edge is generally studied by the well-known Tauc's relation,[32,35] which can be used to find out energy band gap of a material using experimental data:

$$\alpha\, h\nu = B\,(h\nu - E_g)^r \quad (5)$$

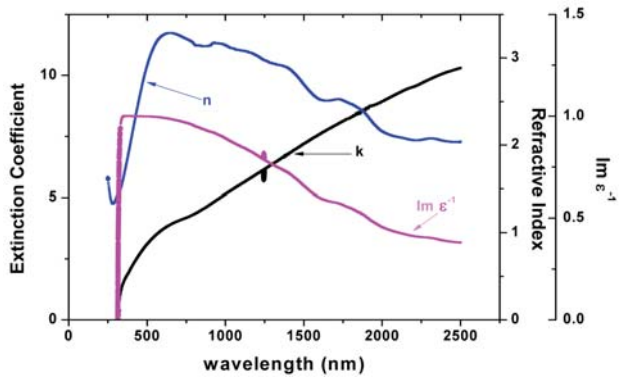

Fig. 3(c) : Spectral dependence of n and *k* of complex refractive index for HfO_2/*Al*/HfO_2 device. Also shown spectral dependence of electron energy-loss function (Im ε^{-1}).

Where α (ν) = 2.303A/d, where A being optical absorbance and d physical thickness of the film, hν the incident photon energy, E_g the energy band gap, B the transition characteristic parameter (independent of photon energy) and r is an index that specifies the type of transition process i.e. 2 for allowed indirect transition, 1/2 for allowed direct transition, 3 for forbidden indirect transition and 3/2 for forbidden direct transition. According to above equation (5), in the vicinity of fundamental absorption edge $(\alpha\, h\nu)^{1/r}$ linearly depends upon photon energy (hν). By extrapolating linear region of the plot to $(\alpha\, h\nu)^{1/r} = 0$, one obtains the value of E_g for respective transition. Such a plot for r = 1/2 (allowed direct transitions) for HfO_2/*Al*/HfO_2 multilayer thin films is shown in Fig. 4(a).

Absorption coefficient in the exponential-edge region is expressed by Urbach relationship: [32,36]

$$\alpha(\nu) = \alpha_o \exp(h\nu / E_u) \quad (6)$$

Where α_o is a constant and E_u is the Urbach energy which characterizes slope of the exponential edge region

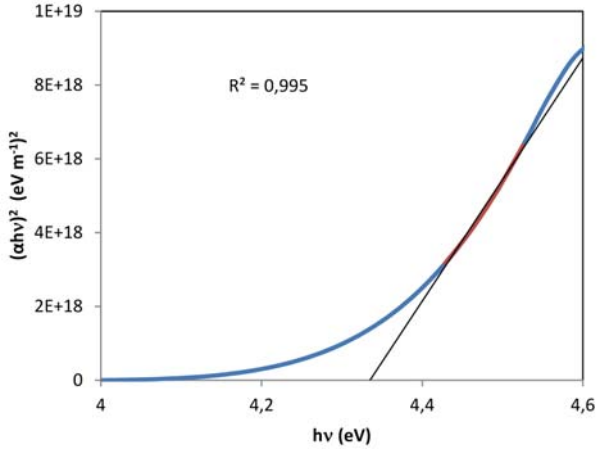

Fig. 4(a): Plot of $(\alpha\, h\nu)^2$ Vs. photon energy h ν for HfO_2/*Al*/HfO_2 device demonstrating energy band gap.

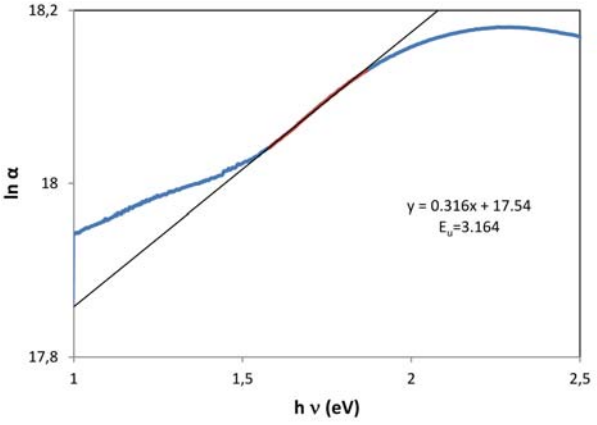

Fig. 4(b): Urbach plot (ln α Vs. photon energy hν) for HfO_2/*Al*/HfO_2 multilayer thin films.

Table 2: Observed optical parameters for present HfO_2/*Al*/HfO_2 multilayer thin films.

Subs. Temp. (°C)	Band gap Eg (eV)	Urbach energy E_u (eV)	Refractive Index n (at λ = 632 nm)	Extinction Coefficient k (at λ = 632nm)
100	4.34	3.164	3.29	3.842

and its inverse gives width of the localized states related to amorphous/disordered phase in the band gap of a thin film. Plot of ln α Vs. photon energy hν for HfO_2 multilayer thin films is represented in Fig. 4(b). The E_u value calculated from slope of the curve is also presented in Table 2.

4. Conclusions

HfO_2/*Al*/HfO_2 multilayer thin films were deposited by electron beam evaporation. XRD patterns show that deposition of *Al* onto HfO_2 led to nano-polycrystals of HfO_2 embedded in a disordered lattice. AFM images reveal a smooth surface (RMS roughness ~3.83 ± 0.42 nm). High optical transmittance of HfO_2/*Al*/HfO_2 multilayer thin films in the UV (~90%) and visible (45%) regions and relatively high reflectance in NIR regions can be useful for some of its applications in energy efficient windows. Moreover high refractive index is an indicative of denser films corresponding to a reduction in film porosity making the device suitable for heat mirror applications. Calculated extinction coefficient illustrates minute optical loss in the visible region, which is an enviable property for heat mirror applications. The direct band gap was found to be ~4.34 eV.

5. Acknowledgements

This work was funded by Higher Education Commission (HEC) Pakistan under pin # 074-2330-Ps4-347 Indigenous Scholarship program. M. Ramzan is thankful to Dr. Nazar Abbas and Waqar Mahmood (Thin Films Labs. CIIT, Islamabad Pakistan) for providing optical characterization facilities.

6. References

1. A. Zakery, S. R. Elliott, *J. Non-Cryst. Solids* **2003**, *330*, 1–12.
2. M. Frumar, J. Jedelsky, B. Frumarova, T. Wagner, M. Hrdlicka, *J. Non-Cryst. Solids* **2003**, *326–327*, 399–404.
3. F. Al-Hazmi, T. Al- Harbi, W. E. Mahmoud, *Mater. Lett*. **2012**, *86*, 28–30.
4. F. A. Al-Agel, *Mater. Lett*. **2013,** *100*, 115–118.
5. J. C. Fan. *Thin Solid Films* **1981**, *80*, 125–136.
6. C. G. Granqvist. *Appl. Opt*. **1981**, *20*, 2606–2615.
7. M. Veszelei, K. Andersson, C. G. Ribbing, K. Jarrendahl, H. Arwin. *Appl. Opt.* **1994**, *33*, 1993–2001.
8. C. M. Lampert, *Sol Energy Mater*. **1981**, *6*, 1–41.
9. H. Kostlin, G. Frank. *Thin Solid Films*. **1982**, *89*, 287–293.
10. P. H. Berning, *Appl. Opt*. **1983**, *22*, 4127–4141.
11. T. Tan, Z. Liu , L. Hongcheng, W. Liu , H. Tian, *Opt. Mater*. **2010**, *32*, 432–435.
12. M. Copel, M. Gribelyuk, E. Gusev, *Appl. Phys. Lett*. **2000**, *76*, 436.
13. G. Wilk, D. Wallace, J. M. Anthony, *J. Appl. Phys*. **2001**, *89*, 5243.
14. T. S. Jeon, J. M. White, D. L. Kwong, *Appl. Phys. Lett*. **2001**, *78*, 368.
15. F. L. Martinez, M. Toledano-Luque, J. J. Gandia, J. Carabe , W. Bohne, J. Roehrich, E. Strub, I. Martil, *J. Phys. D: Appl. Phys*. **2007**, *40*, 5256–5265.
16. M. Balog, M. Schieber, M. Michman, S. Patai, *Thin Solid Films*. **1977**, *41*, 247.
17. S. M. Edlou, A. Smajkiewicz, G. A. Al-Jumaily, *Appl. Opt*. **1993**, *32*, 5601.
18. M. F. Al-Kuhaili. *Opt. Mater.* **2004**, *27*, 383–387.
19. N. Selvakumar, H. C. Barshilia, K. S. Rajam, A. Biswas, *Sol. Energy Mater. Sol. Cells*, **2010**, *94*, 1412–1420.
20. N. Selvakumar, H. C. Barshilia, K. S. Rajam, *Nanostruc. Mater. Elect. Energy Envir. Appl*. **2010**, 319–324.
21. Salwan K. Al-Ani. *Iraqi J. Appl. Phys*. **2008**, *4*, 17–23.
22. JCPDS database, International Center for Powder Diffraction Data, PA, **1999**.
23. S. Joydip, R. K Sahoo, C. D. Mukherjee, *Mater. Lett*. **2012**, *83*, 84–87.
24. M. Senthilkumar, N. K. Sahoo, S. Thakur, R. B. Tokas, *Appl. Surf. Sci*. **2005**, *245*, 114.
25. D. Kalhor, R. Zahiri, A. Ebrahimzad. *World Appl. Sci. J.,* **2009**, *7,* 17–22.
26. Y. S. Kim, J. H. Park, D. H. Choi, H. S. Jang, J. H. Lee, H. J. Park, J. I. Choi, D. H. Ju, J. Y. Lee and Daeil Kim. *Appl. Surf. Sci.* **2007**, *254*, 1524–1527.
27. S. Kunduy, S. Hazray, S. Banerjeey, M. K. Sanyaly, S. K. Mandalz, S. Chaudhuriz and A. K. Pal, *J. Phys. D: Appl. Phys.* **1998**, *31*, L73–L77.
28. C. J. Lefaux, J. A. Zimberlin, A. V. Dobrynin, P. T. Mather, *J. Polymer Sci. Part B: Polymer Phys.* **2004**, *42*, 3654–3666.
29. A. Alaeddin, A. Saif, N. Ramli, P. Poopalan, *Jordan J. Phys*. **2010**, *3*, 61–68.
30. A. M. Al-Shukri, *Desalination* **2007**, *209*, 290–297.
31. M. Kojima, F. Takahashi, K. Kinoshita, T. Nishibe, M. Ichidate, *Thin Solid Films* **2001**, *392*, 349–354.
32. M. Ramzan, M. F. Wasiq, A. M. Rana, S. Ali, M. Y. Nadeem, *Appl. Surf. Sci*. **2013**, *283*, 617–622.
33. G. H. Dobrikov, M. M. Rassovska, N. M. Andreev, S. I. Boyadzhiev, K. A. Gesheva, T. M. Ivanova, P. S. Sharlandjiev,

D. I. Nazarowa, *Thin Solid Films* **2009**, *518*, 1091–1094.
34. W. Zhenguo, C. Xun, C. Qiulong, L. Liuhe, *Vacuum* **2006**, *80*, 438–443.
35. W. Zhang, J. Fu, X. Shen, Y. Chen, S. Dai, F. Chen, J. Li, T. Xu *J. Non-Cryst. Solids*. **2013**, *377*, 191–194.
36. F. Urbach, *Phys. Rev*. **1953**, *92*, 1324.

Povzetek

V članku poročamo o večplastnih tankih filmih HfO_2/Al/HfO_2, primernih za toplotna zrcala. Pripravili smo jih na steklenem substratu z naparevanjem z elektronskim curkom. Rezultati rentgenske praškovne analize filmov, pripravljenih pri temperaturi substrata 100 °C, kažejo na nano-polikristalite HfO_2 nameščene v neurejeni mreži. Mikroskopija na atomsko silo (AFM) je pokazala, da imajo plasti HfO_2/Al/HfO_2 gladko površino, ki je primerna za optična toplotna zrcala. Študija optičnih lastnosti z UV-VIS spektroskopijo je pokazala, da se prepustnost HfO_2/Al/HfO_2 zmanjšuje od UV do VIS območja in nato rahlo povečuje v NIR območju. Meritve refleksije izkazujejo nasprotni trend. Izračunali smo tudi vrednosti lomnega količnika, ekstinkcijskega koeficienta, energijske špranje (širina prepovedanega energijskega pasu) in Urbachove energije. Vrednosti za energijsko špranjo in Urbachovo energijo sta 4,34 eV in 3,164 eV. Opazovali smo tudi skupno oscilacijsko izgubo energije toplotnih zrcal.